SUPPORTING INFORMATION FOR

Computational study of the resistance shown by the Subtype B / HIV-1 protease to currently known inhibitors

Alessandro Genoni [(a,b)], Giulia Morra [(a)], Kenneth M. Merz Jr. [(b)], Giorgio Colombo [(a)]

(a) Istituto di Chimica del Riconoscimento Molecolare, CNR, Via Mario Bianco 9, 20131, Milano, Italy.

(b) Quantum Theory Project, University of Florida, P.O. Box 118435, Gainesville, Florida, 32611, USA.

Communication Propensity Values

Table S1 - Average communication propensity value for each simulation.

	BLAI	BV6	BMDR
APO	0.0181	0.0168	0.0262
INDINAVIR	0.0211	0.0162	0.0204
NELFINAVIR	0.0147	0.0202	0.0287
RITRONAVIR	0.0147	0.0151	0.0264
TL-3	0.0104	0.0143	0.0297
SUBSTRATE	0.0140	0.0170	0.0299

Table S2 - Minimum communication propensity value for each simulation.

	BLAI	BV6	BMDR
APO	0.0010	0.0012	0.0010
INDINAVIR	0.0011	0.0008	0.0009
NELFINAVIR	0.0009	0.0011	0.0011
RITRONAVIR	0.0008	0.0008	0.0011
TL-3	0.0008	0.0010	0.0011
SUBSTRATE	0.0008	0.0008	0.0009

Table S3 - Maximum communication propensity value for each simulation.

	BLAI	BV6	BMDR
APO	0.0744	0.0613	0.2395
INDINAVIR	0.1147	0.0735	0.1178
NELFINAVIR	0.0795	0.0933	0.3271
RITRONAVIR	0.0845	0.0758	0.1778
TL-3	0.0453	0.0851	0.2360
SUBSTRATE	0.0700	0.1083	0.1834

Table S4 – Comparison between the dynamical spaces of the MD simulations performed (RWSIP Values).

		BLAI						BV6						BMDR					
		APO	IND	NFV	RIT	TL3	Sub	APO	IND	NFV	RIT	TL3	Sub	APO	IND	NFV	RIT	TL3	Sub
BLAI	APO	1.00																	
	IND	0.59	1.00																
	NFV	0.43	0.44	1.00															
	RIT	0.48	0.39	0.46	1.00														
	TL3	0.40	0.38	0.71	0.44	1.00													
	Sub	0.46	0.35	0.43	0.62	0.41	1.00												
BV6	APO	0.43	0.41	0.41	0.44	0.43	0.39	1.00											
	IND	0.41	0.38	0.42	0.41	0.40	0.37	0.66	1.00										
	NFV	0.36	0.35	0.45	0.37	0.48	0.36	0.38	0.34	1.00									
	RIT	0.42	0.35	0.38	0.39	0.37	0.34	0.70	0.64	0.32	1.00								
	TL3	0.35	0.34	0.47	0.45	0.46	0.41	0.37	0.34	0.62	0.32	1.00							
	Sub	0.41	0.36	0.44	0.45	0.44	0.41	0.42	0.39	0.54	0.37	0.56	1.00						
BMDR	APO	0.40	0.26	0.46	0.42	0.43	0.32	0.44	0.37	0.30	0.43	0.29	0.35	1.00					
	IND	0.41	0.32	0.39	0.41	0.36	0.35	0.67	0.70	0.35	0.62	0.33	0.39	0.40	1.00				
	NFV	0.35	0.29	0.34	0.39	0.41	0.31	0.47	0.40	0.32	0.42	0.31	0.37	0.46	0.47	1.00			
	RIT	0.45	0.32	0.39	0.40	0.31	0.33	0.60	0.60	0.31	0.49	0.28	0.34	0.35	0.61	0.36	1.00		
	TL3	0.41	0.32	0.38	0.49	0.40	0.41	0.43	0.33	0.45	0.39	0.46	0.51	0.47	0.41	0.52	0.34	1.00	
	Sub	0.44	0.31	0.40	0.43	0.38	0.33	0.61	0.54	0.37	0.50	0.34	0.40	0.43	0.63	0.36	0.63	0.63	1.00

RMSd Profiles

Figure S1. Root Mean Square Deviation (RMSd) of the $C\alpha$ atoms with respect to starting structure for the BLAI_APO, BLAI_IND and BLAI_NFV simulations (equilibration and production phase).

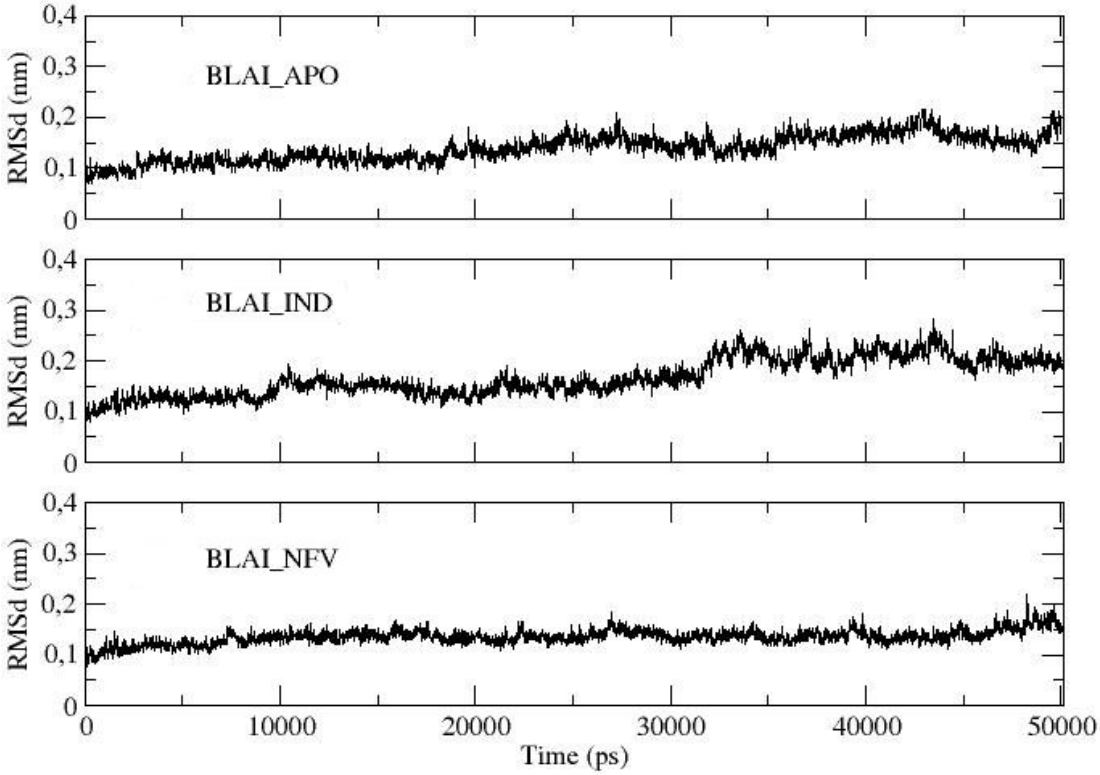

Figure S2. Root Mean Square Deviation (RMSd) of the $C\alpha$ atoms with respect to the starting structure for the BLAI_RIT, BLAI_TL3 and BLAI_SUB simulations (equilibration and production phase).

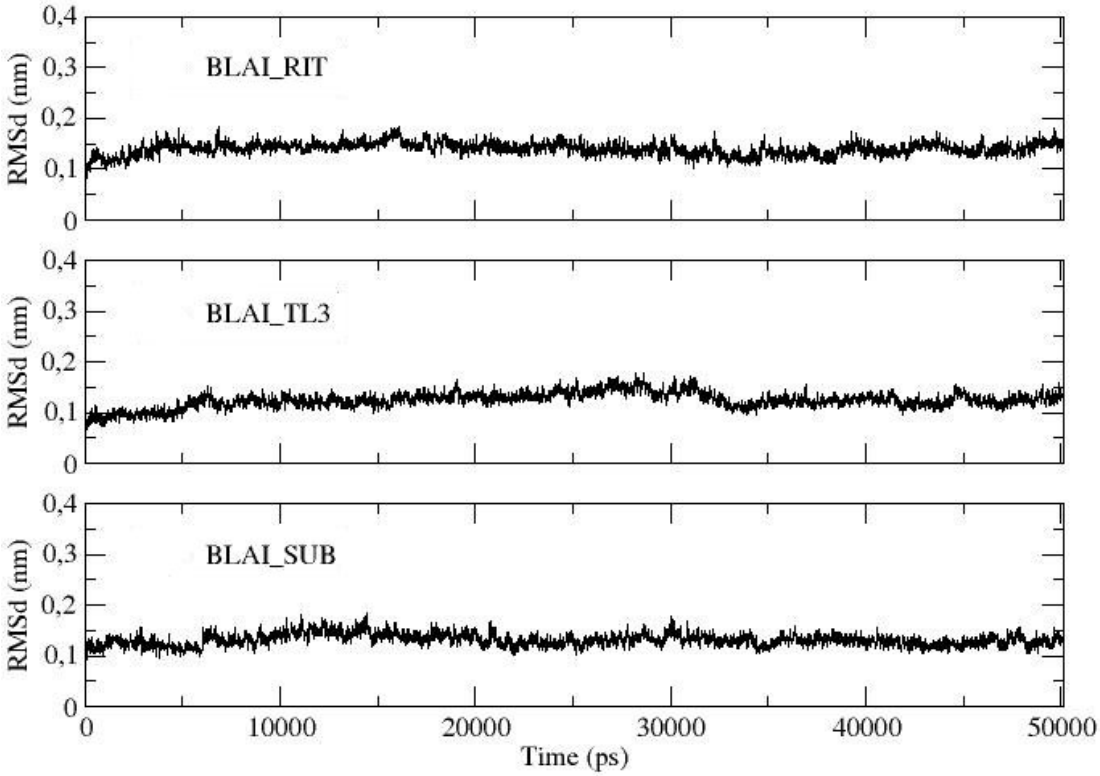

Figure S3. Root Mean Square Deviation (RMSd) of the $C\alpha$ atoms with respect to the starting structure for the BV6_APO, BV6_IND and BV6_NFV simulations (equilibration and production phase).

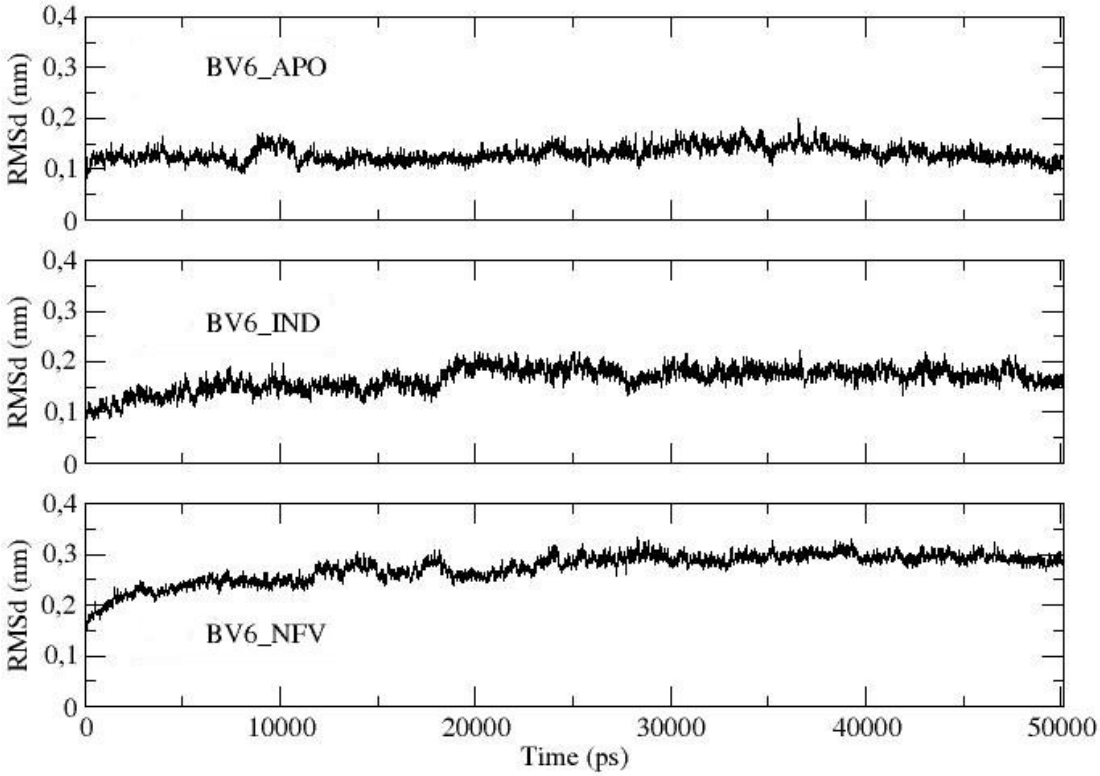

Figure S4. Root Mean Square Deviation (RMSd) of the $C\alpha$ atoms with respect to the starting structure for the BV6_RIT, BV6_TL3 and BV6_SUB simulations (equilibration and production phase).

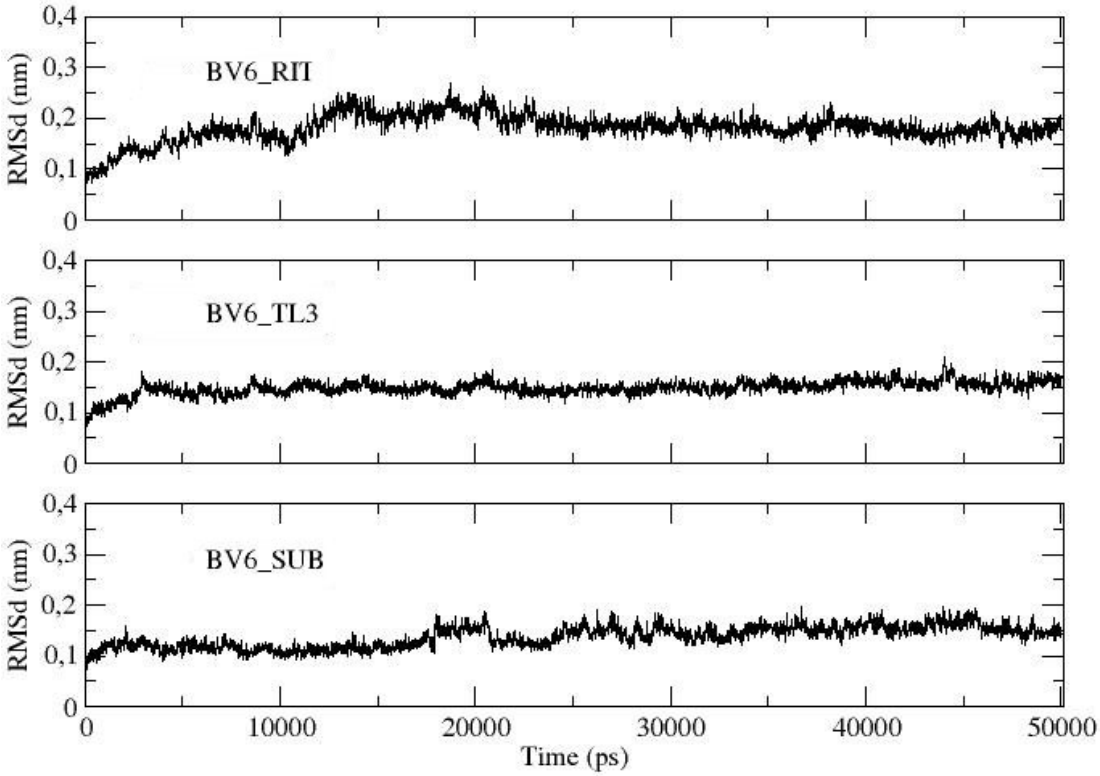

Figure S5. Root Mean Square Deviation (RMSd) of the $C\alpha$ atoms with respect to the starting structure for the BMDR_APO, BMDR_IND and BMDR_NFV simulations (equilibration and production phase).

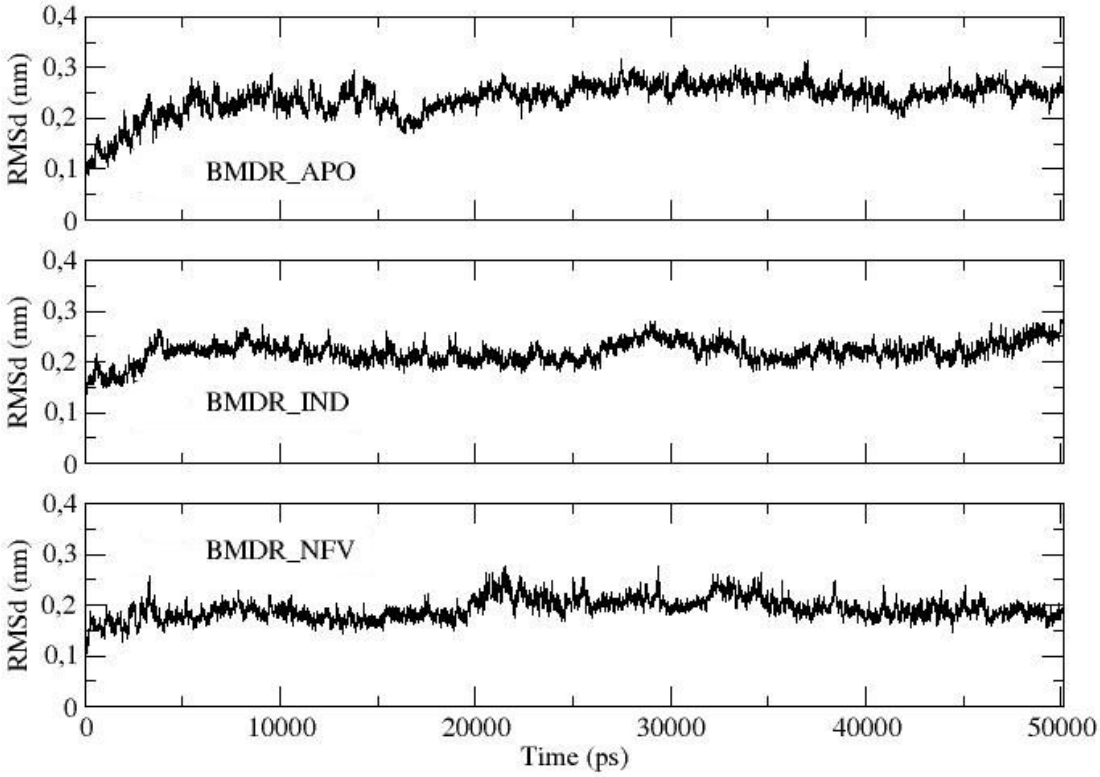

Figure S6. Root Mean Square Deviation (RMSd) of the $C\alpha$ atoms with respect to the starting structure for the BMDR_RIT, BMDR_TL3 and BMDR_SUB simulations (equilibration and production phase).

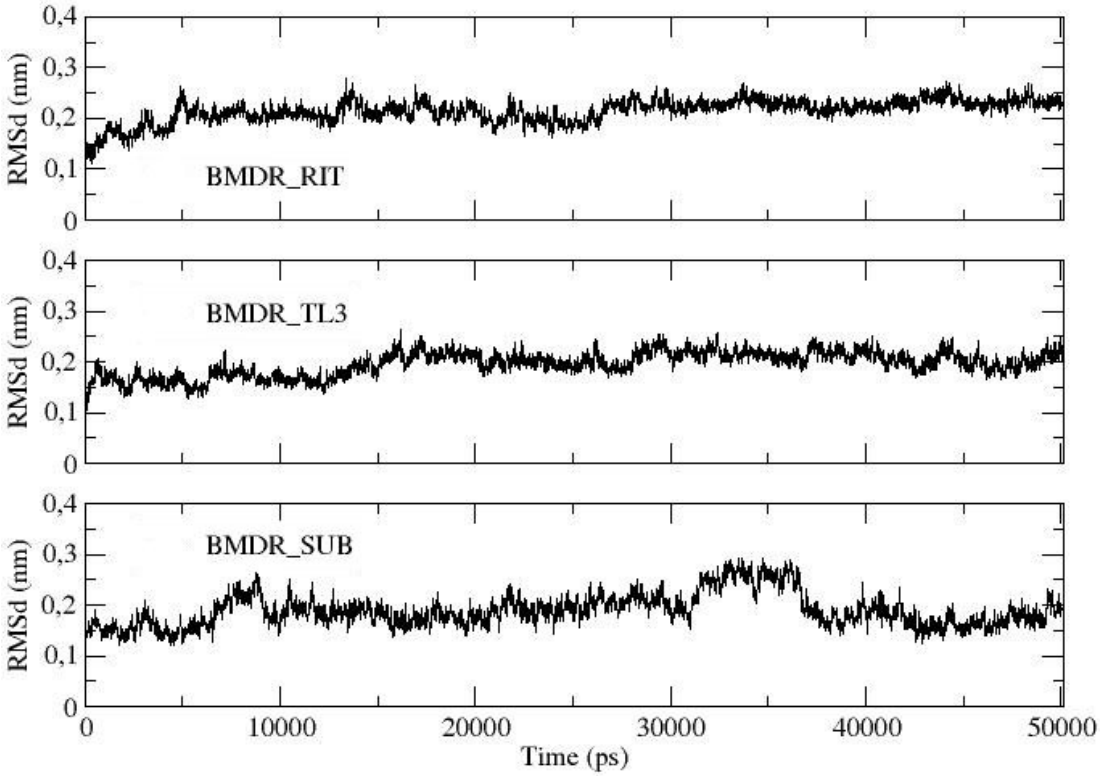

ILCP Figures

Figure S7. Intrinsic Long-Range Communication Propensities (ILCPs) for each residue of the BLAI HIV-1 Protease (namely, the wild type LAI) in all the simulations performed (δ = 15 Å). The red arrows indicate the active site residues in the protease sequence.

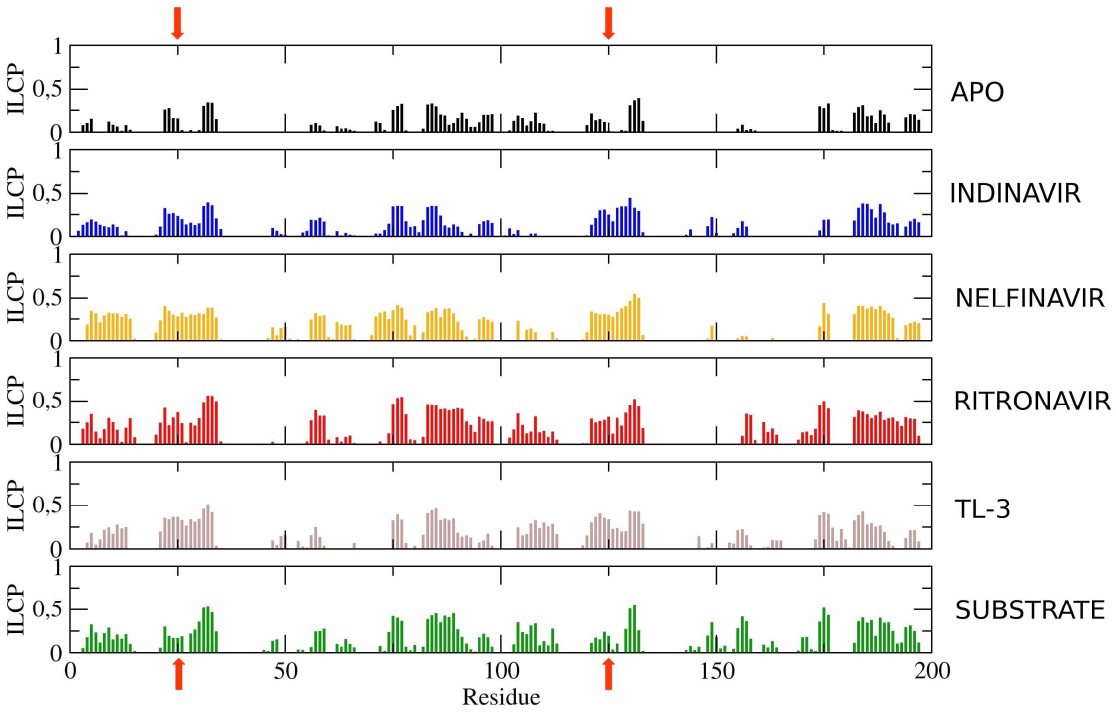

Figure S8. Intrinsic Long-Range Communication Propensities (ILCPs) for each residue of the BLAI HIV-1 Protease (namely, the wild type LAI) in all the simulations performed (δ = 20 Å). The red arrows indicate the active site residues in the protease sequence.

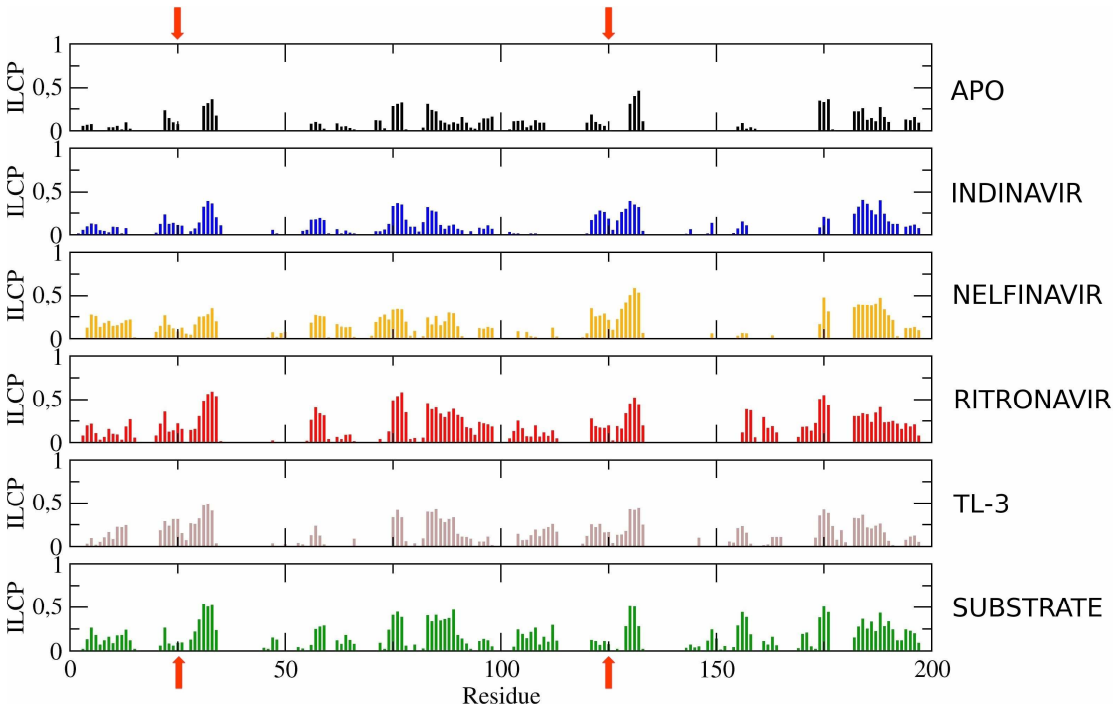

Figure S9. Intrinsic Long-Range Communication Propensities (ILCPs) for each residue of the BV6 mutant (namely, the pseudo-V6 mutant) in all the simulations performed (δ = 15 Å). The red arrows indicate the active site residues in the protease sequence.

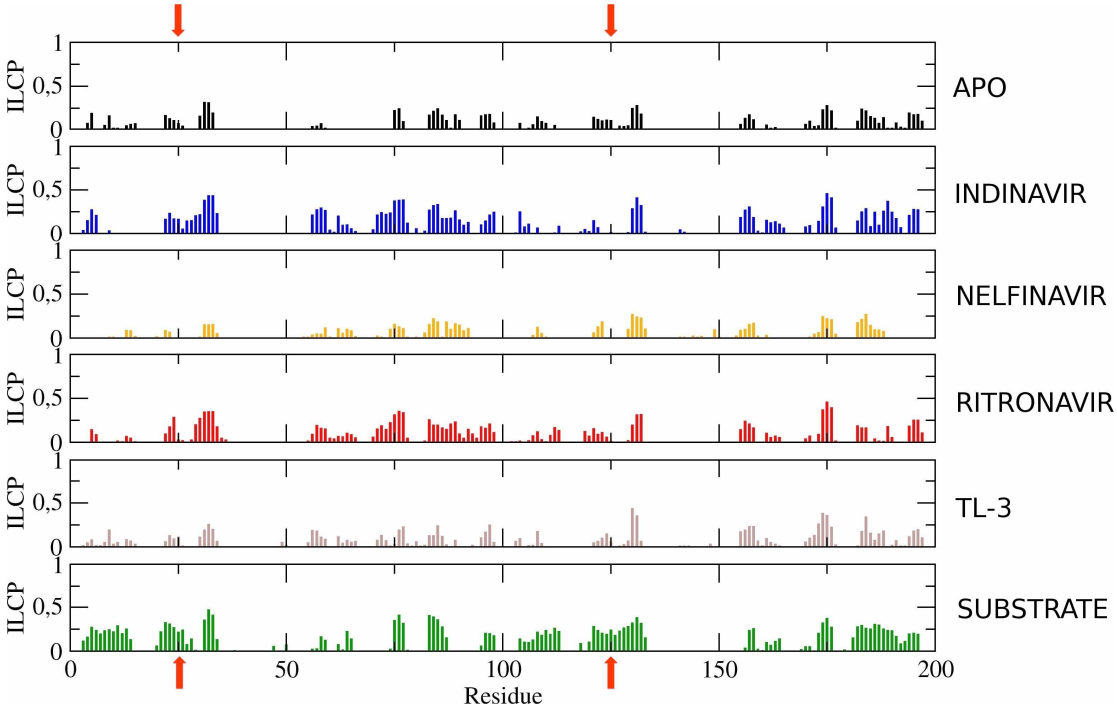

Figure S10. Intrinsic Long-Range Communication Propensities (ILCPs) for each residue of the BV6 mutant (namely, the pseudo-V6 mutant) in all the simulations performed (δ = 20 Å). The red arrows indicate the active site residues in the protease sequence.

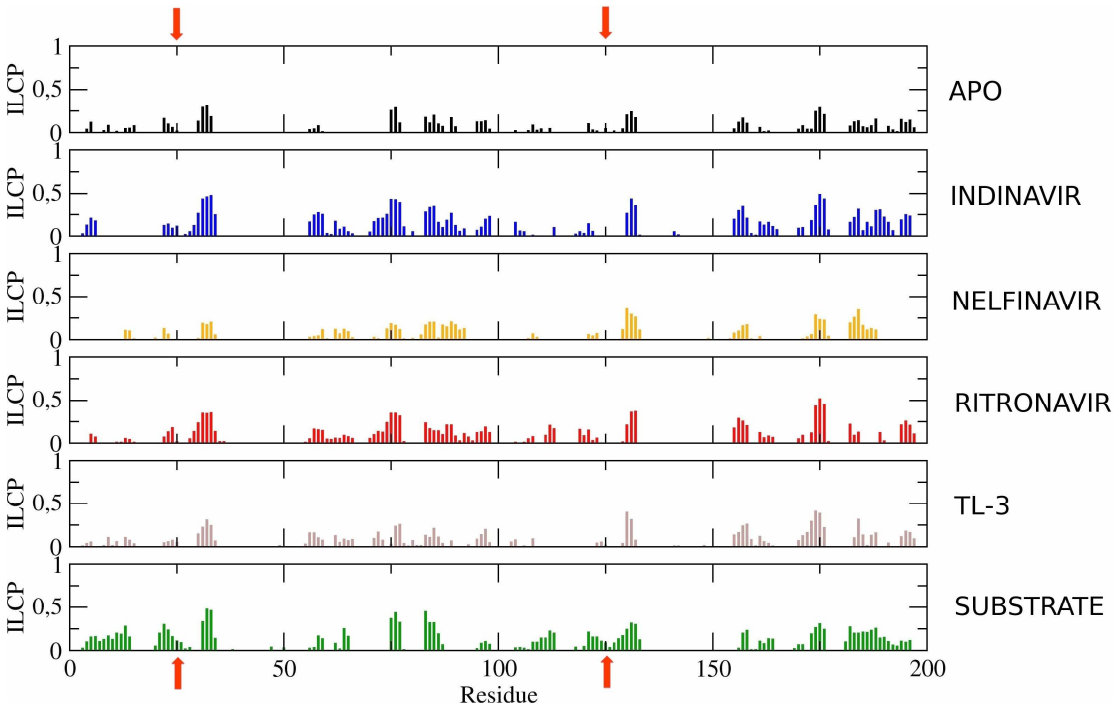

Figure S11. Intrinsic Long-Range Communication Propensities (ILCPs) for each residue of the BMDR mutant (namely, the MDR 769 mutant) in all the simulations performed (δ = 10 Å). The red arrows indicate the active site residues in the protease sequence.

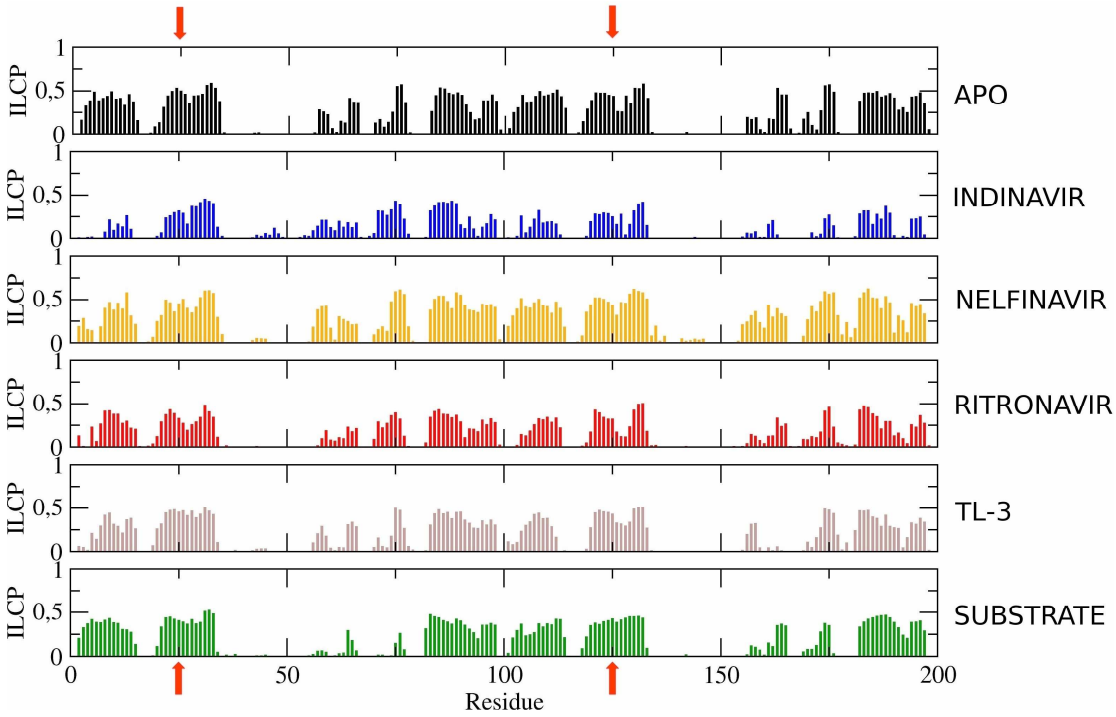

Figure S12. Intrinsic Long-Range Communication Propensities (ILCPs) for each residue of the BMDR mutant (namely, the MDR 769 mutant) in all the simulations performed (δ = 15 Å). The red arrows indicate the active site residues in the protease sequence.

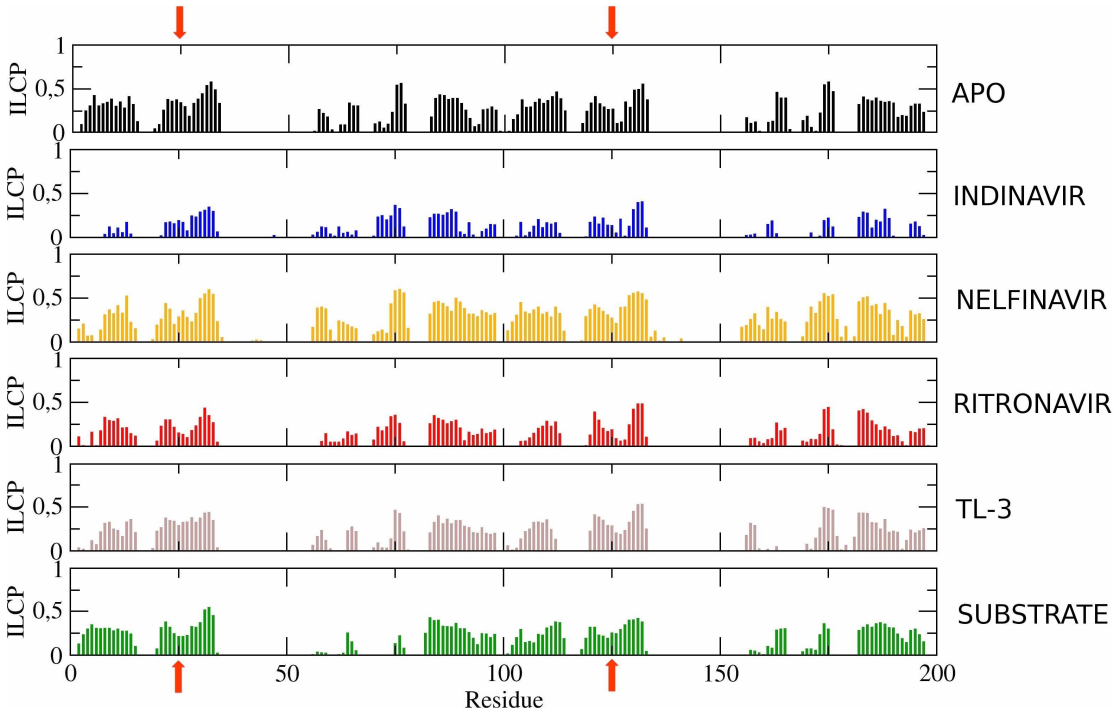

Figure S13. Intrinsic Long-Range Communication Propensities (ILCPs) for each residue of the BMDR mutant (namely, the MDR 769 mutant) in all the simulations performed (δ = 20 Å). The red arrows indicate the active site residues in the protease sequence.

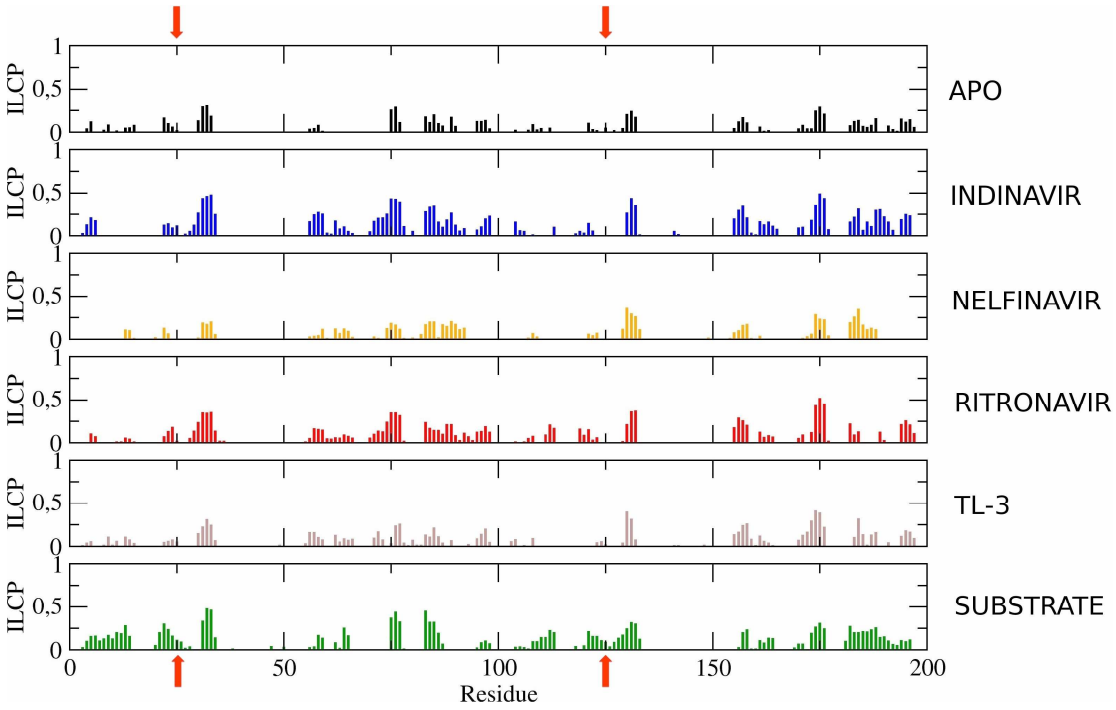

RMSf Profiles

Figure S14. RMSf (*Root Mean Square Fluctuation*) profiles corresponding to the first eigenvector of the covariance matrix for BLAI_APO, BV6_APO and BMDR_APO.

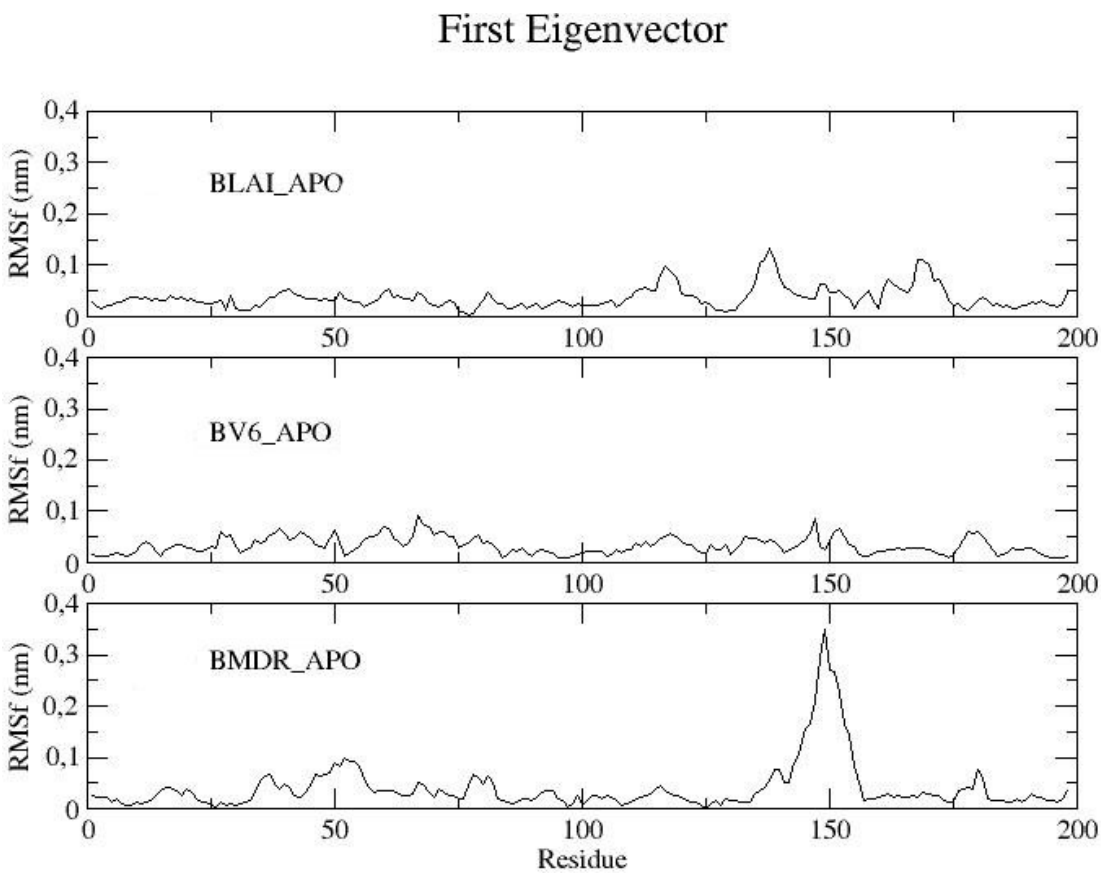

Figure S15. RMSf (*Root Mean Square Fluctuation*) profiles corresponding to the first eigenvector of the covariance matrix for BLAI_IND, BV6_IND and BMDR_IND.

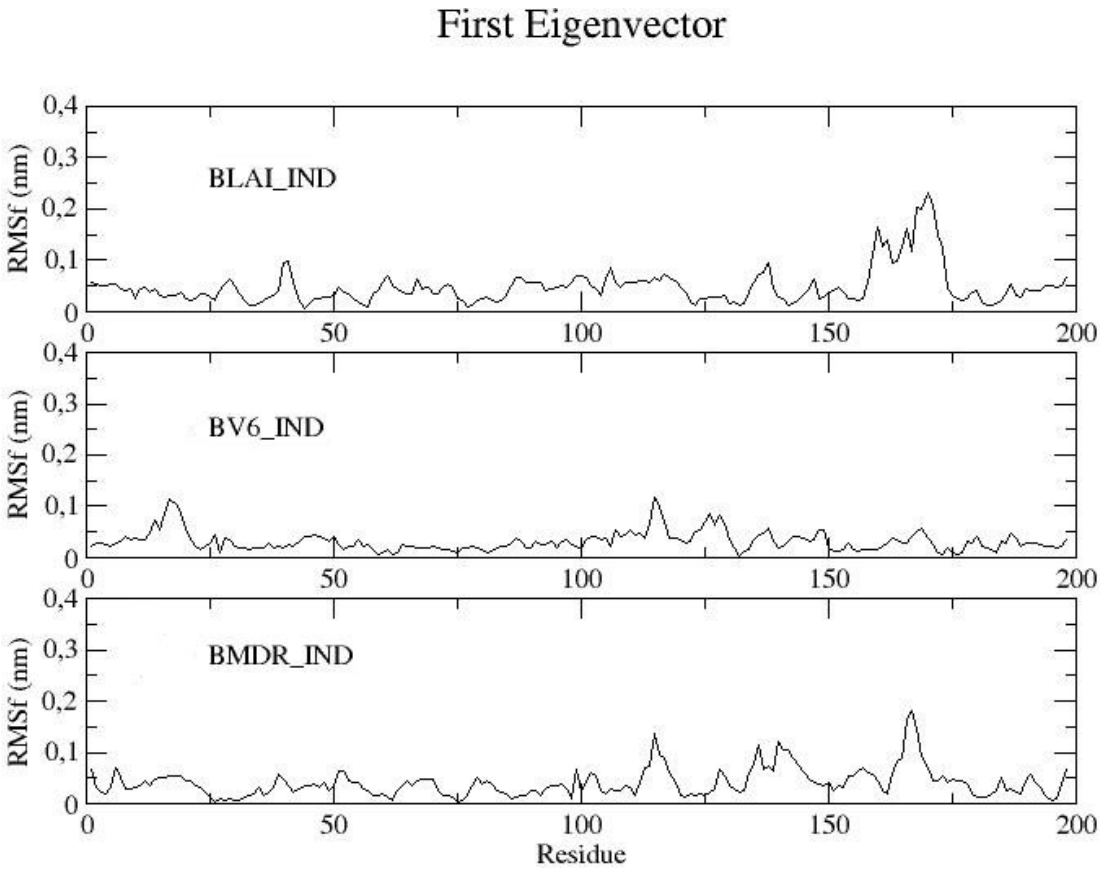

Figure S16. RMSf (*Root Mean Square Fluctuation*) profiles corresponding to the first eigenvector of the covariance matrix for BLAI_NFV, BV6_NFV and BMDR_NFV.

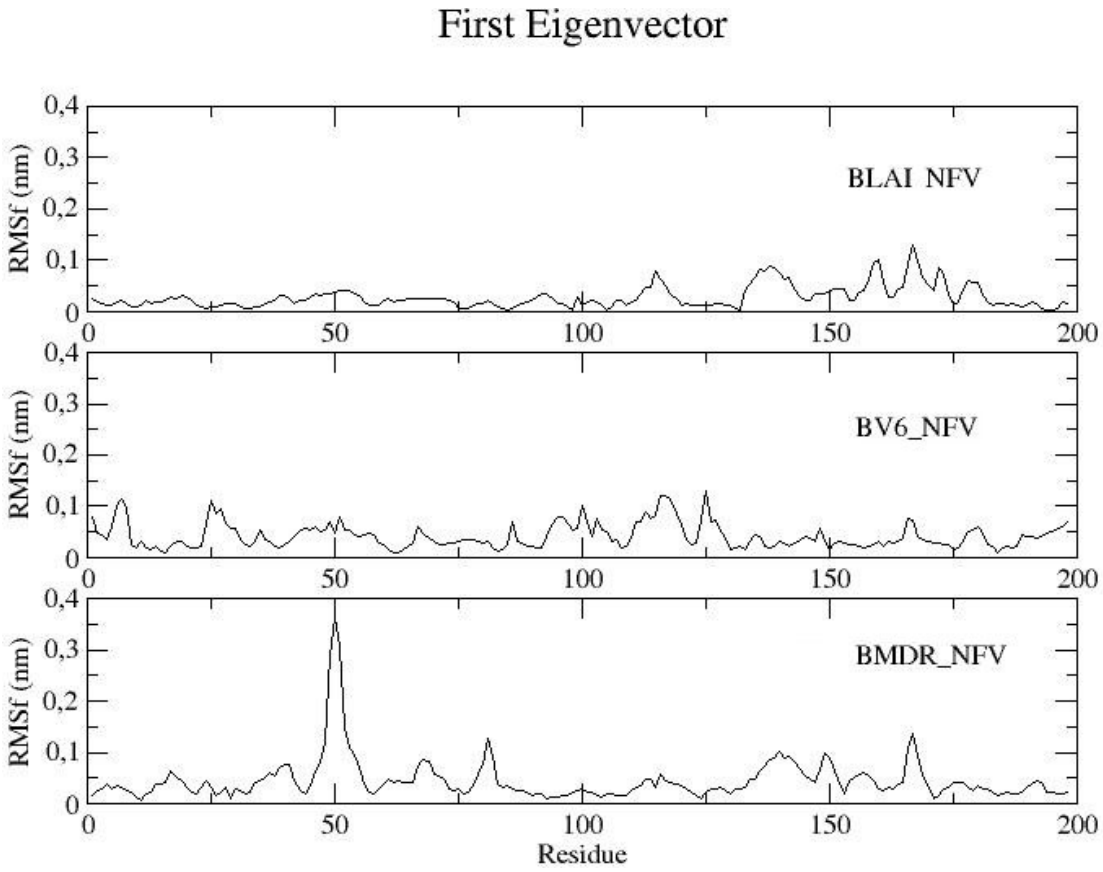

Figure S17. RMSf (*Root Mean Square Fluctuation*) profiles corresponding to the first eigenvector of the covariance matrix for BLAI_RIT, BV6_RIT and BMDR_RIT.

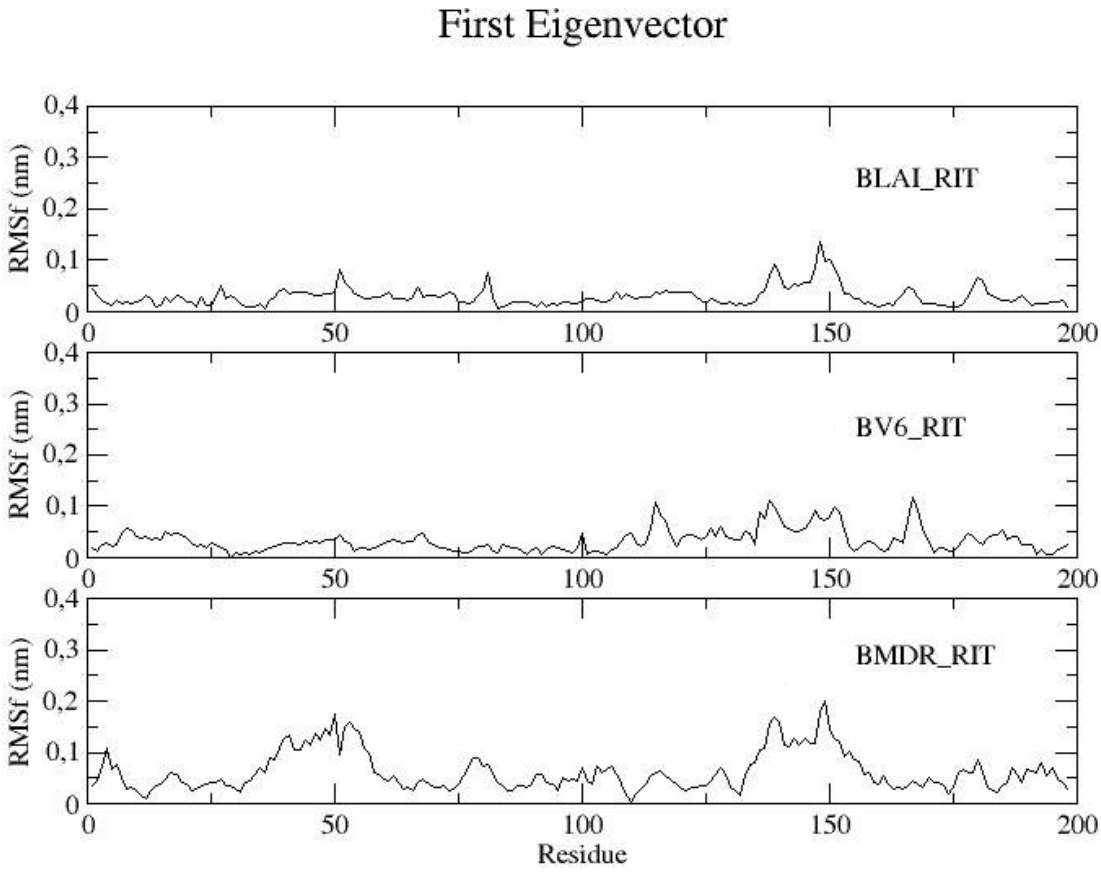

Figure S18. RMSf (*Root Mean Square Fluctuation*) profiles corresponding to the first eigenvector of the covariance matrix for BLAI_TL3, BV6_TL3 and BMDR_TL3.

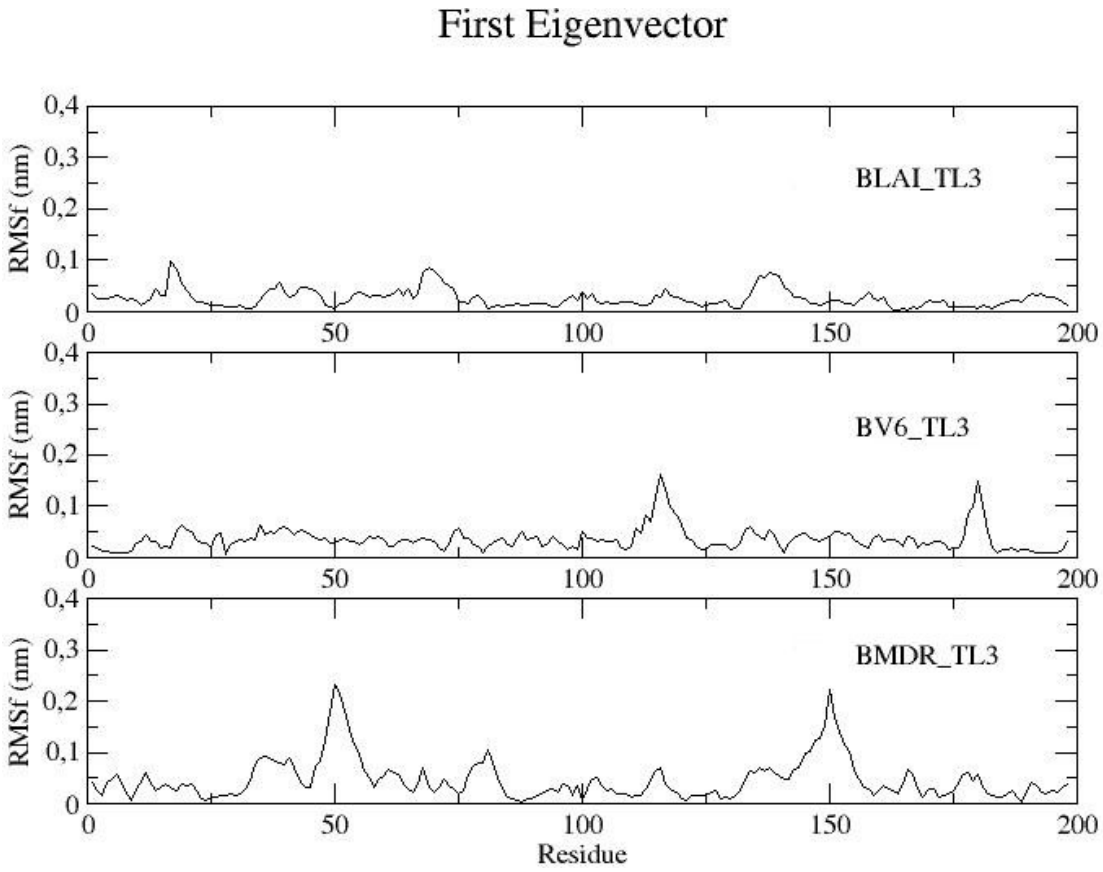

Figure S19. RMSf (*Root Mean Square Fluctuation*) profiles corresponding to the first eigenvector of the covariance matrix for BLAI_SUB, BV6_SUB and BMDR_SUB.

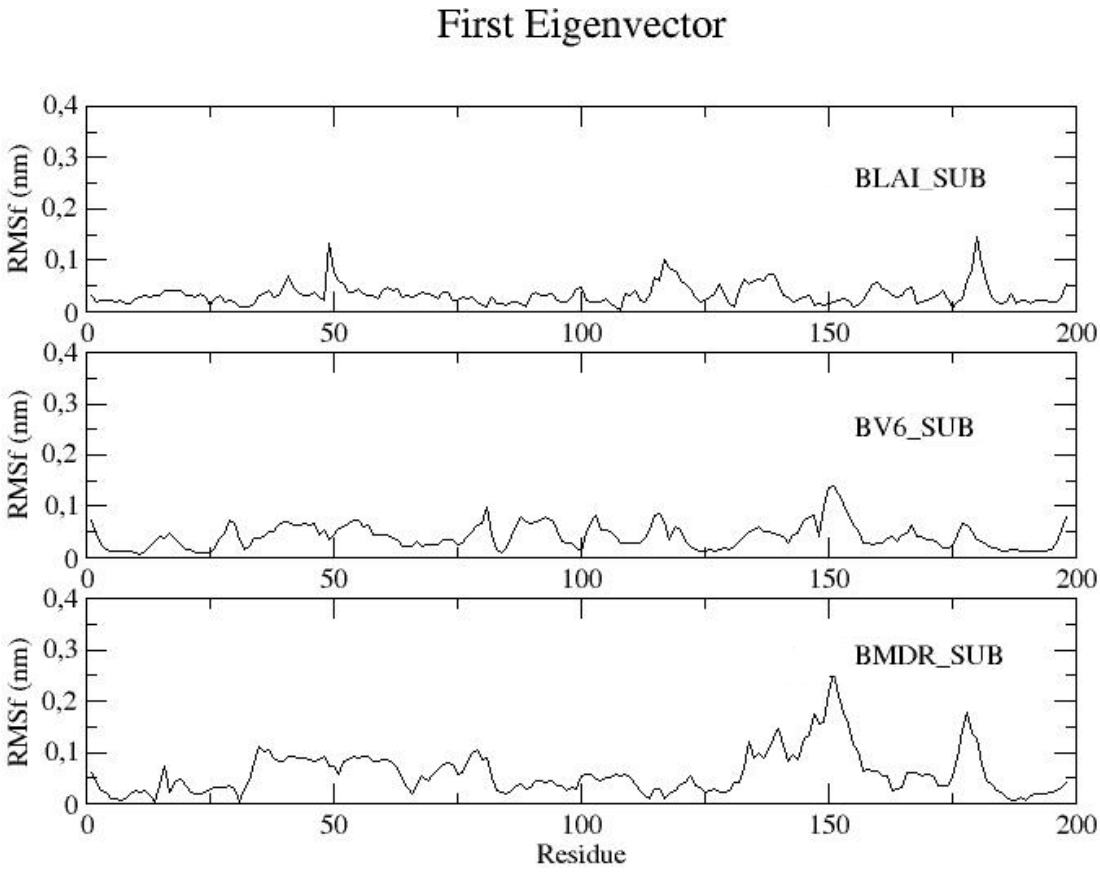

Figure S20. RMSf (*Root Mean Square Fluctuation*) profiles corresponding to the second eigenvector of the covariance matrix for BLAI_APO, BV6_APO and BMDR_APO.

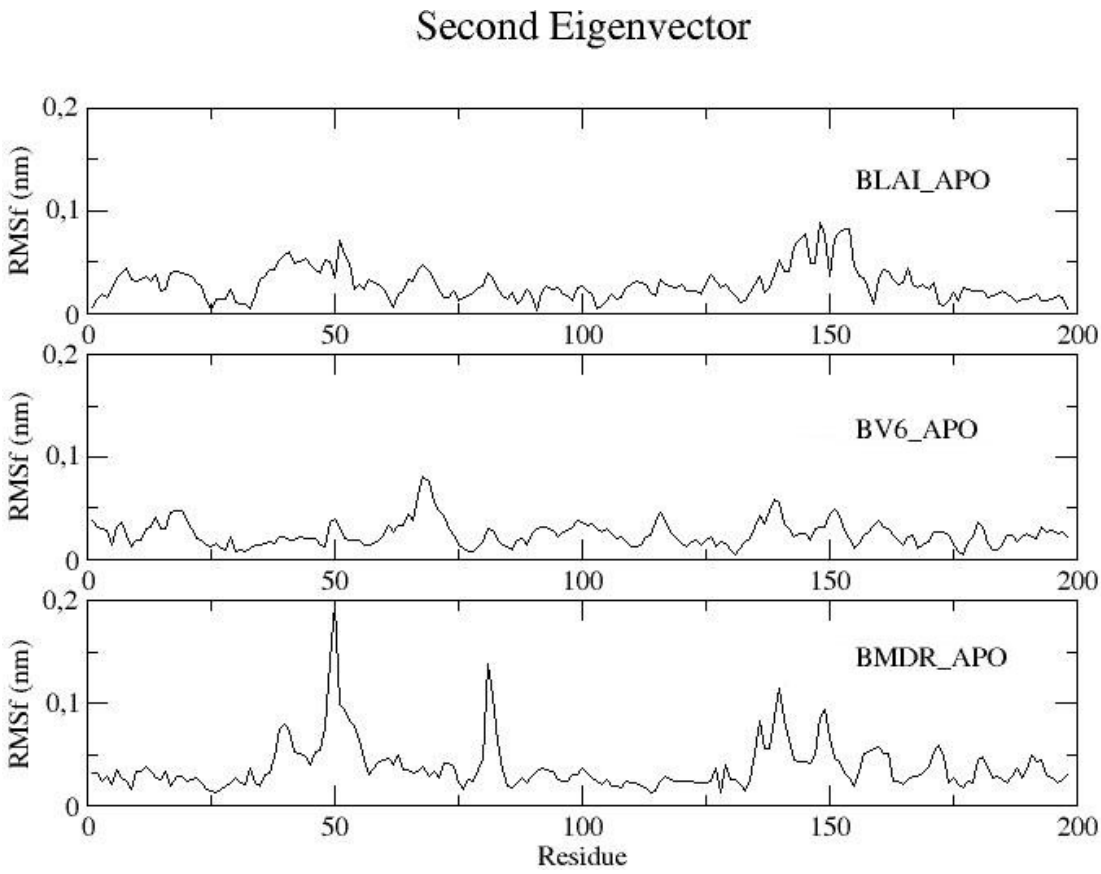

Figure S21. RMSf (*Root Mean Square Fluctuation*) profiles corresponding to the second eigenvector of the covariance matrix for BLAI_IND, BV6_IND and BMDR_IND.

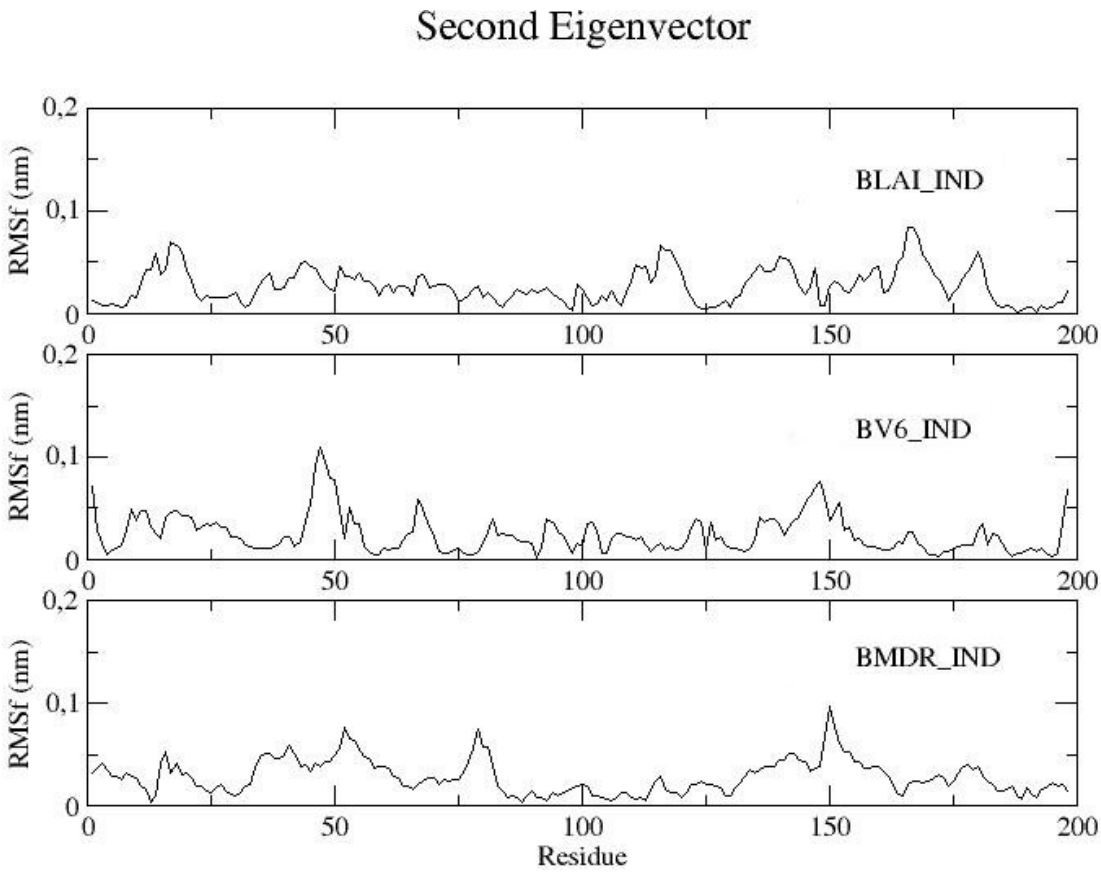

Figure S22. RMSf (*Root Mean Square Fluctuation*) profiles corresponding to the second eigenvector of the covariance matrix for BLAI_NFV, BV6_NFV and BMDR_NFV.

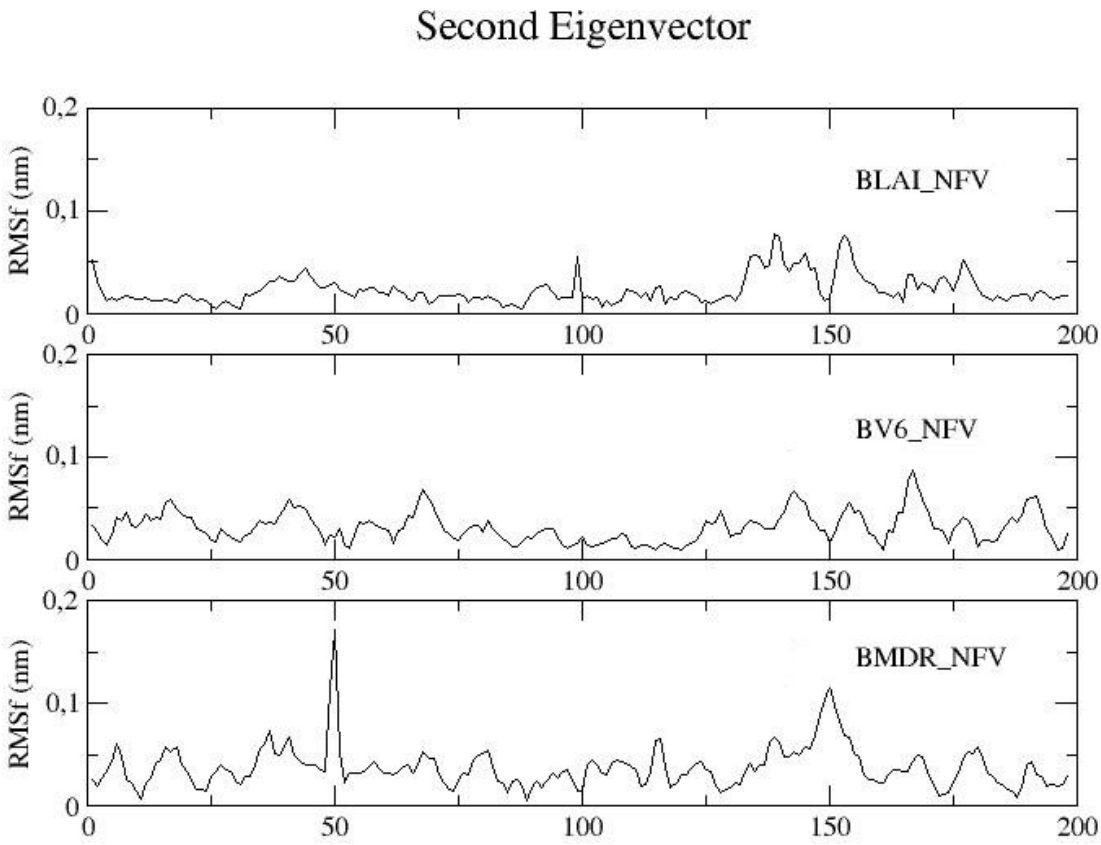

Figure S23. RMSf (*Root Mean Square Fluctuation*) profiles corresponding to the second eigenvector of the covariance matrix for BLAI_RIT, BV6_RIT and BMDR_RIT.

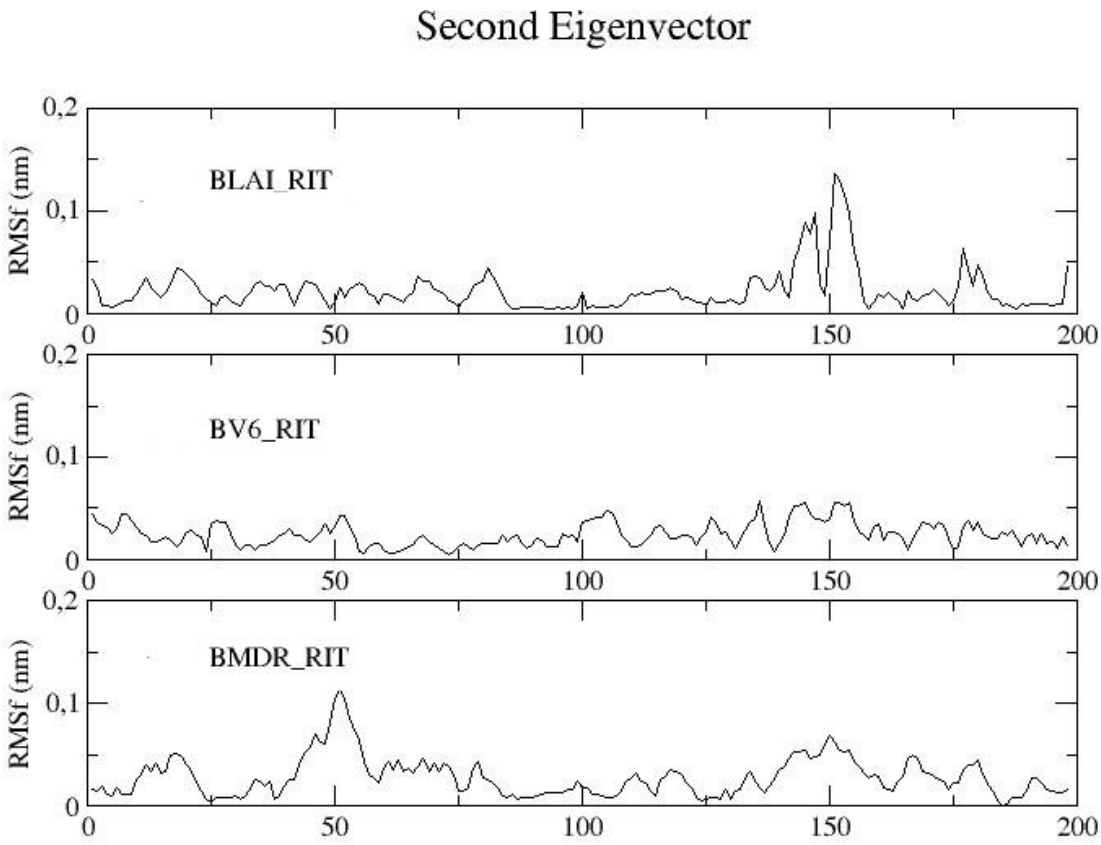

Figure S24. RMSf (*Root Mean Square Fluctuation*) profiles corresponding to the second eigenvector of the covariance matrix for BLAI_TL3, BV6_TL3 and BMDR_TL3.

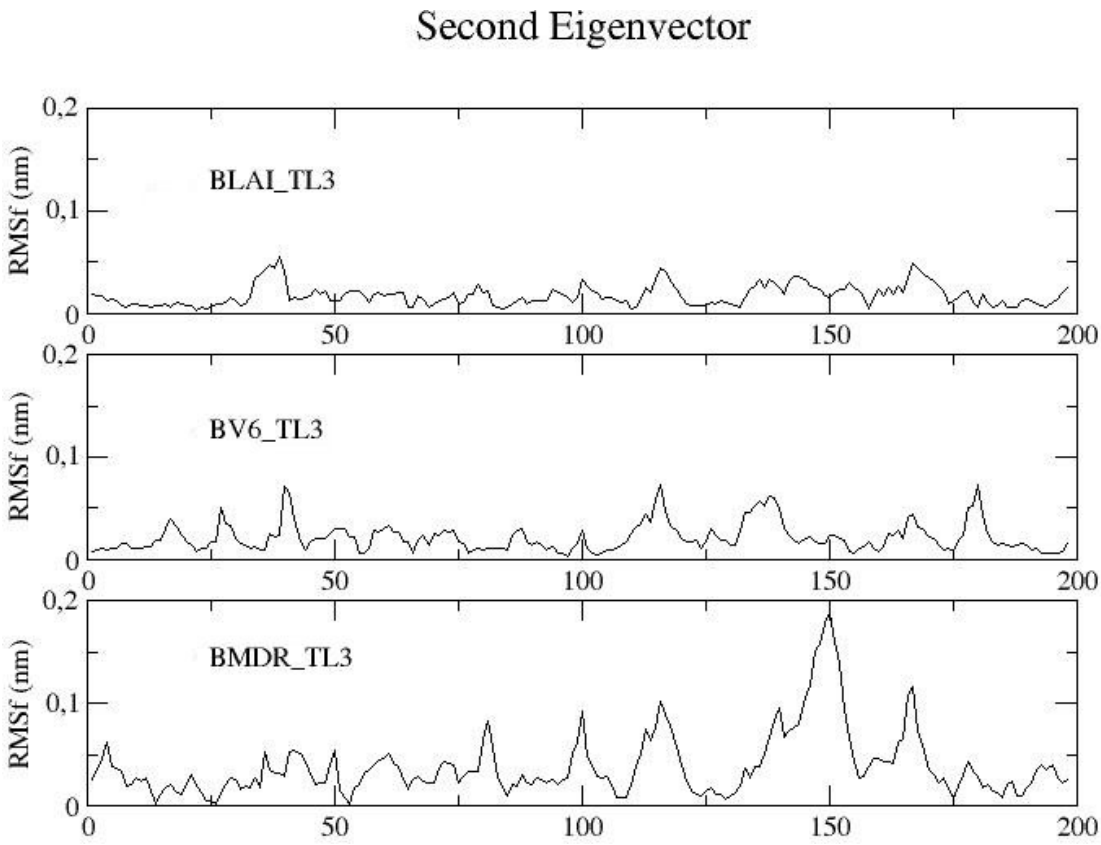

Figure S25. RMSf (*Root Mean Square Fluctuation*) profiles corresponding to the second eigenvector of the covariance matrix for BLAI_SUB, BV6_SUB and BMDR_SUB.

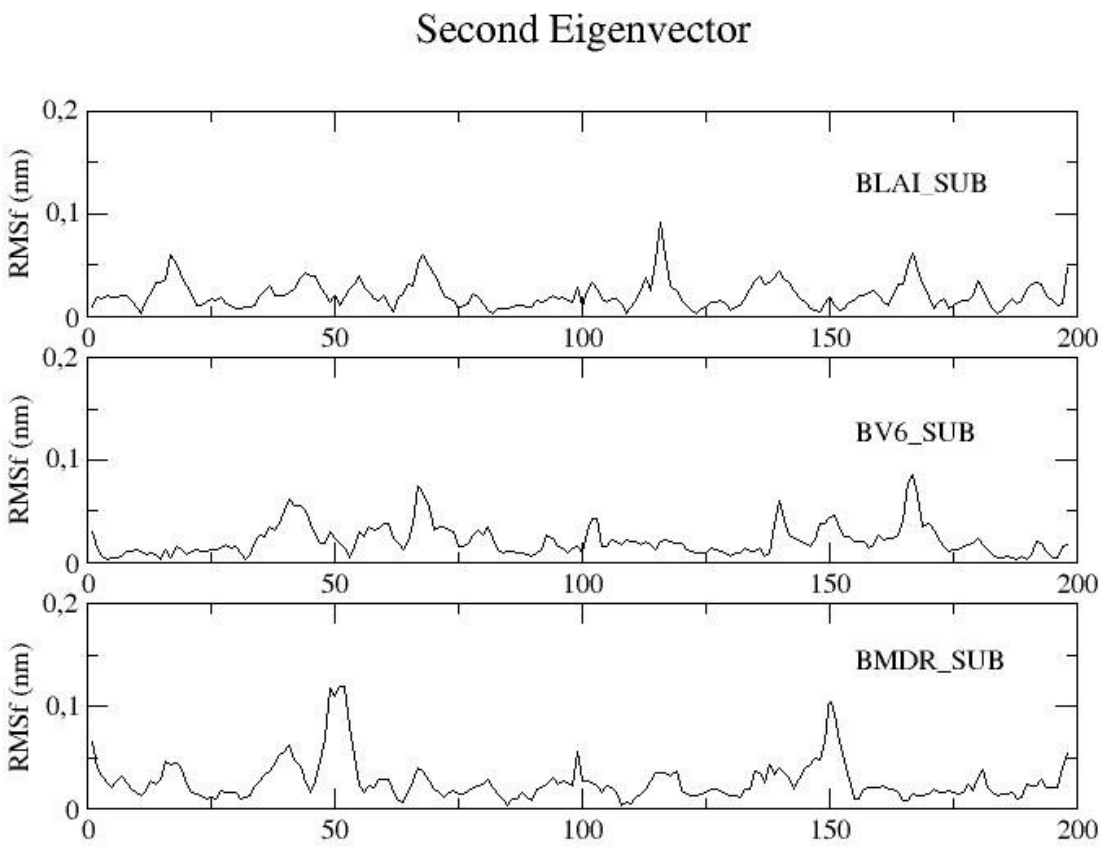

Figure S26. RMSf (*Root Mean Square Fluctuation*) profiles corresponding to the third eigenvector of the covariance matrix for BLAI_APO, BV6_APO and BMDR_APO.

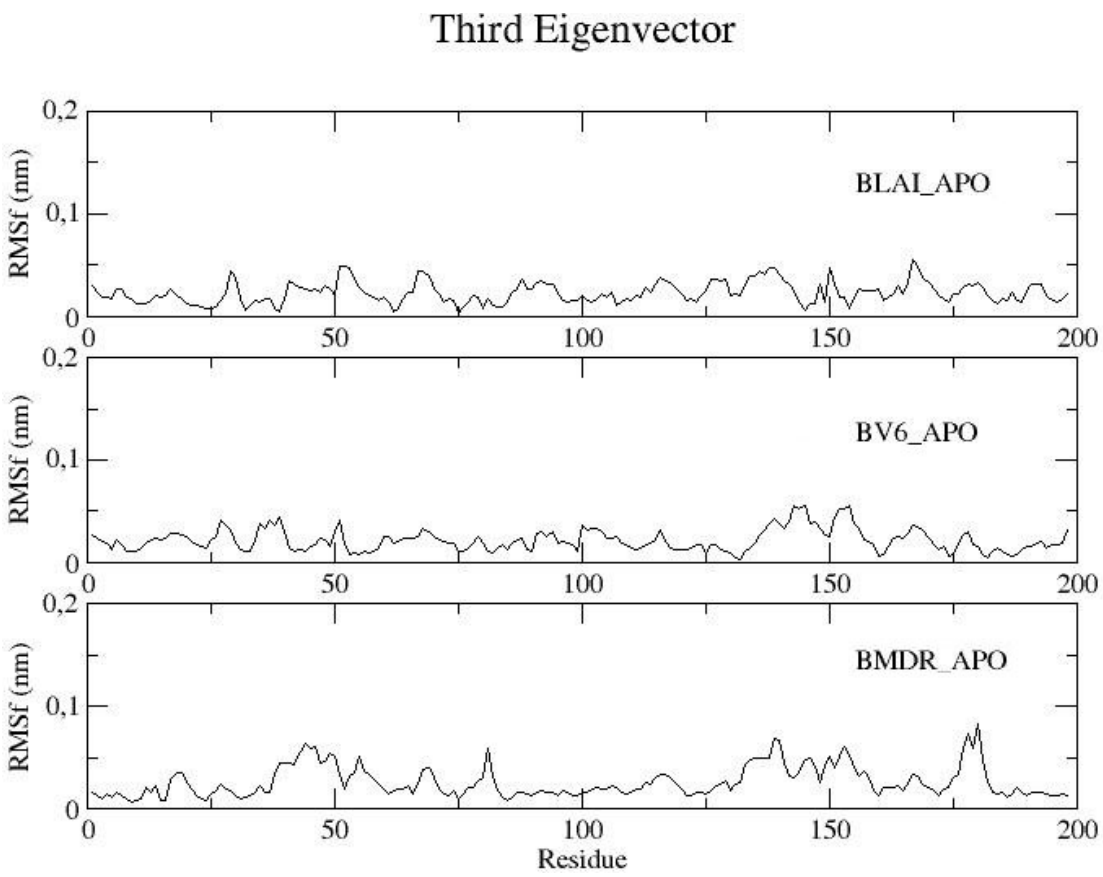

Figure S27. RMSf (*Root Mean Square Fluctuation*) profiles corresponding to the third eigenvector of the covariance matrix for BLAI_IND, BV6_IND and BMDR_IND.

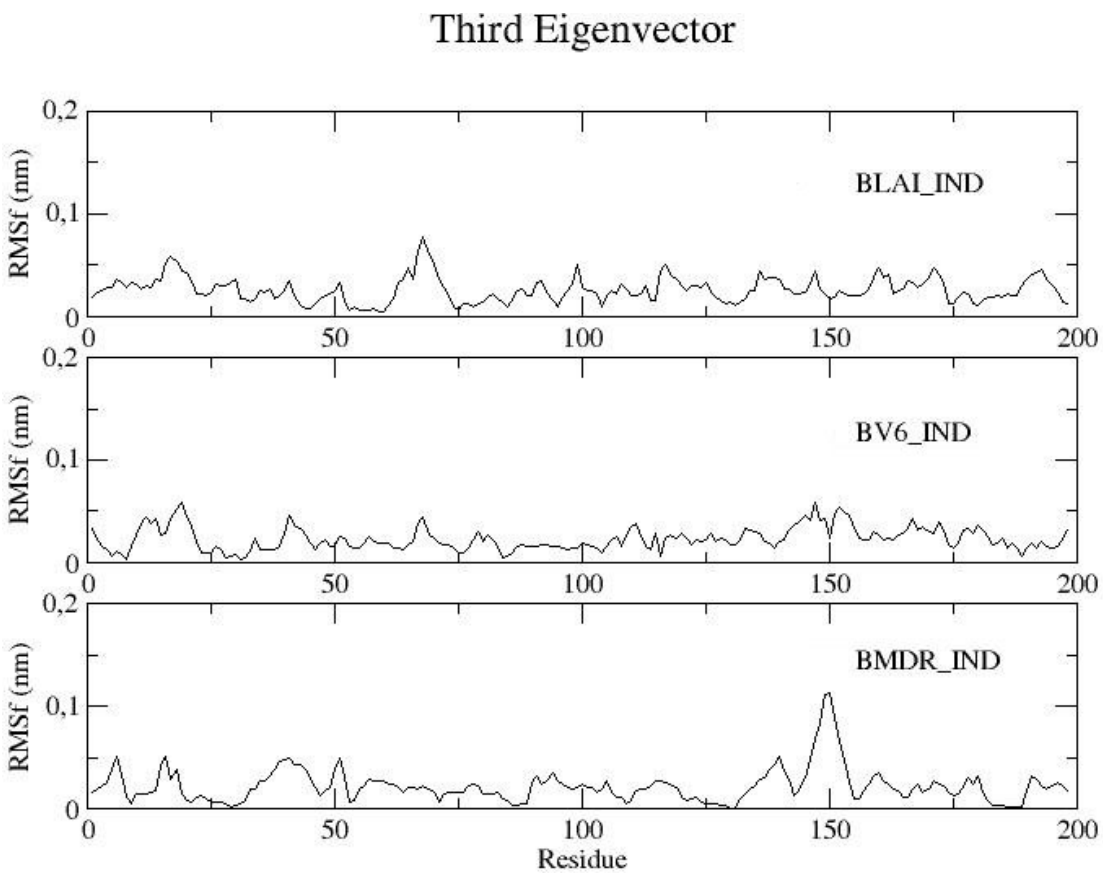

Figure S28. RMSf (*Root Mean Square Fluctuation*) profiles corresponding to the third eigenvector of the covariance matrix for BLAI_NFV, BV6_NFV and BMDR_NFV.

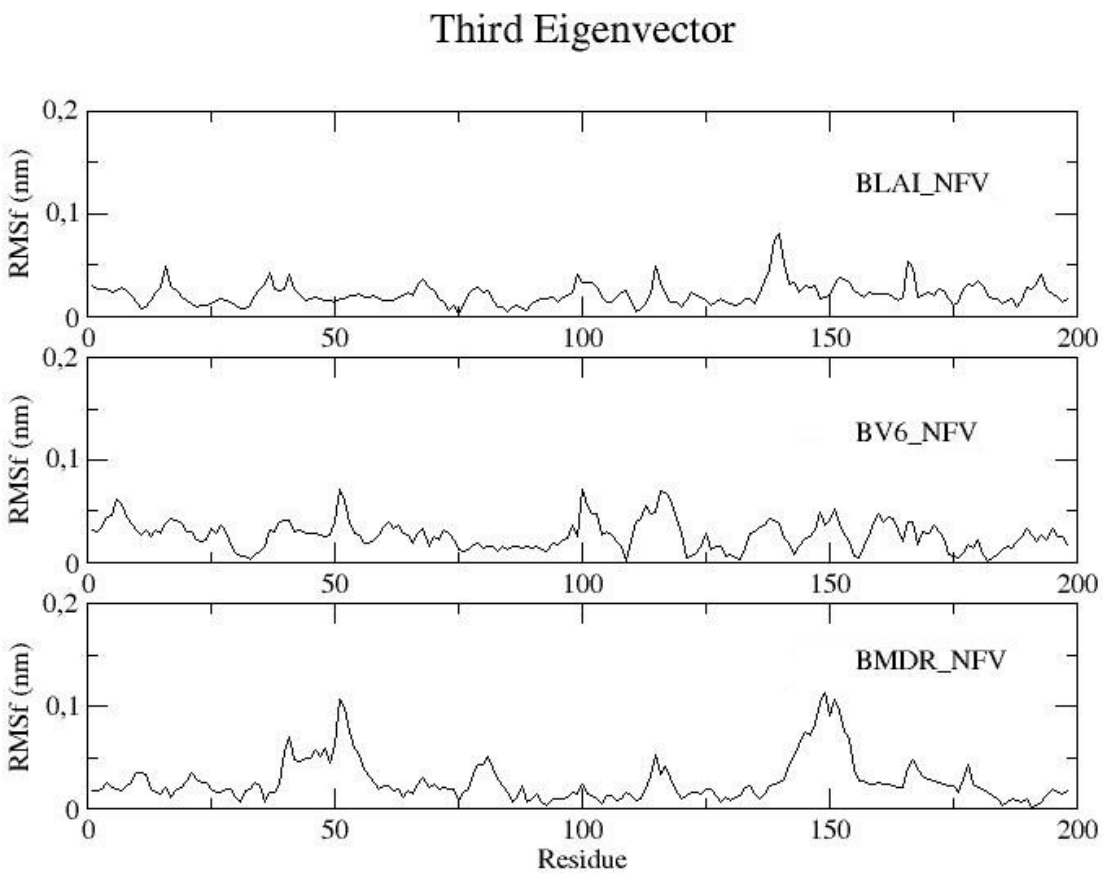

Figure S29. RMSf (*Root Mean Square Fluctuation*) profiles corresponding to the third eigenvector of the covariance matrix for BLAI_RIT, BV6_RIT and BMDR_RIT.

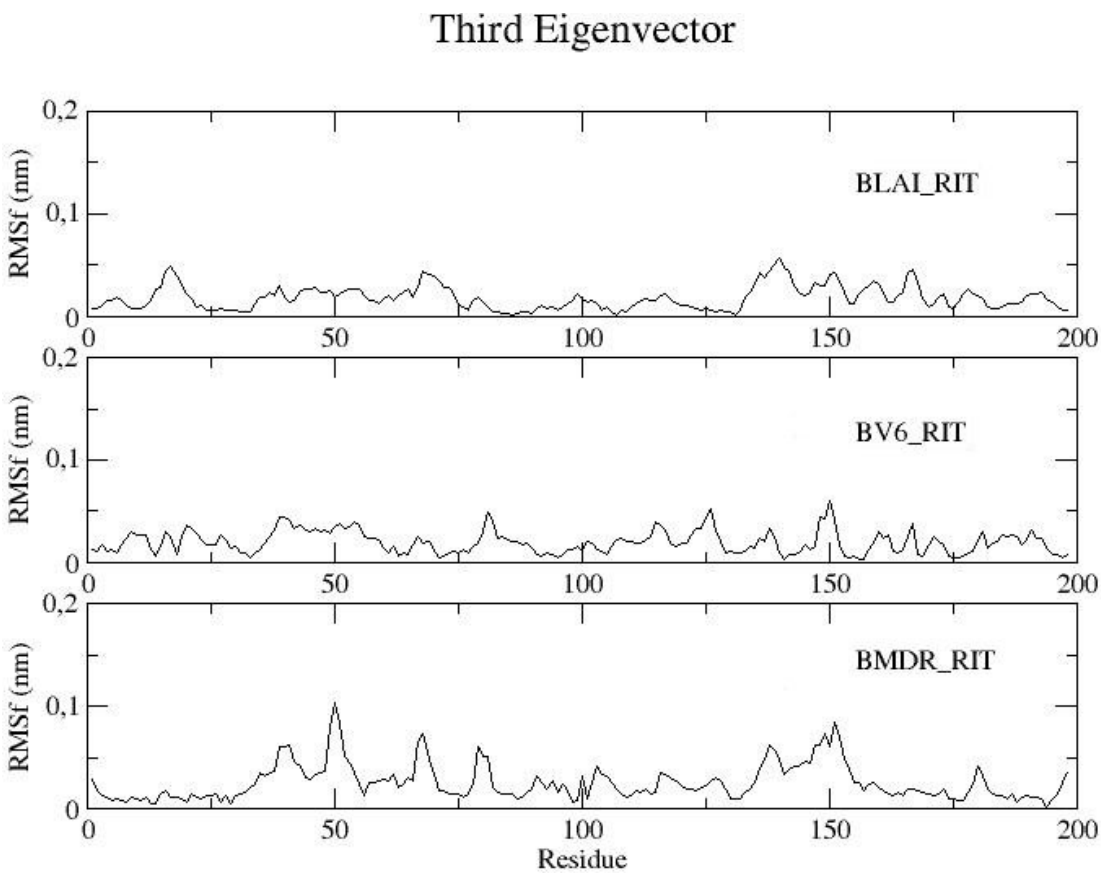

Figure S30. RMSf (*Root Mean Square Fluctuation*) profiles corresponding to the third eigenvector of the covariance matrix for BLAI_TL3, BV6_TL3 and BMDR_TL3.

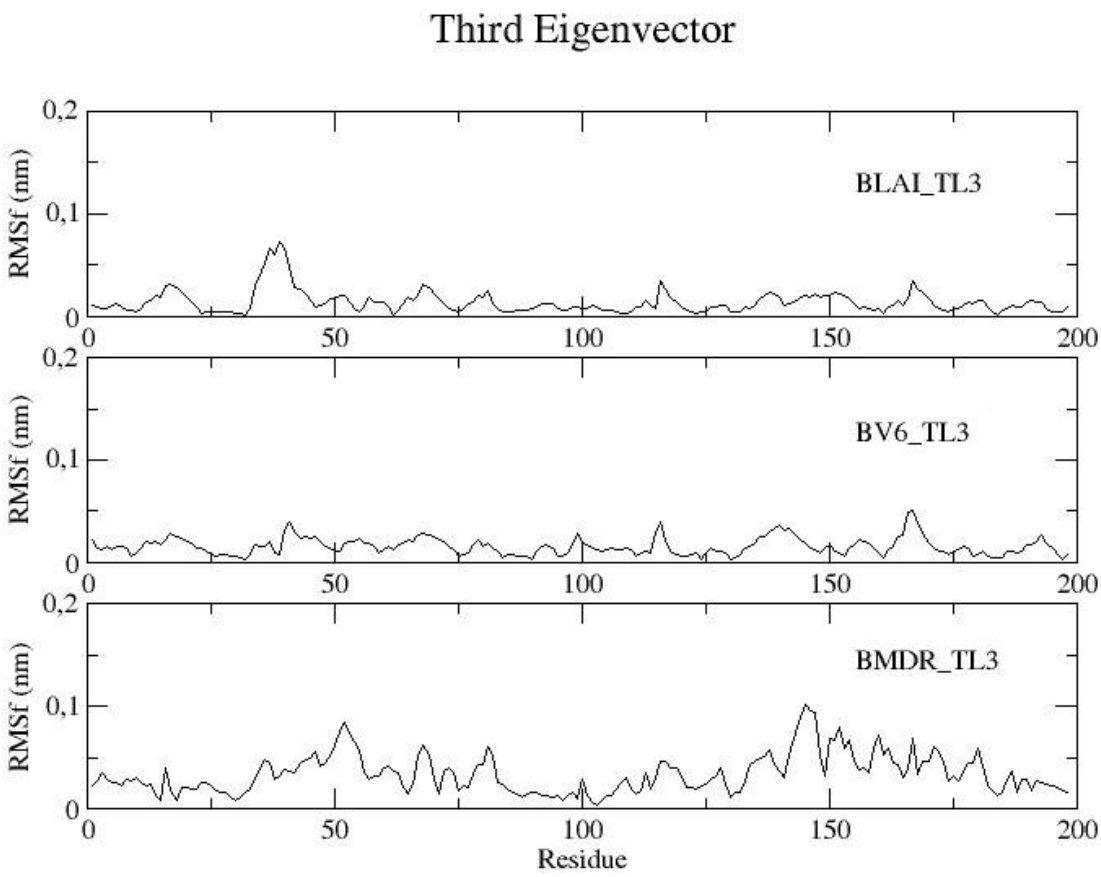

Figure S31. RMSf (*Root Mean Square Fluctuation*) profiles corresponding to the third eigenvector of the covariance matrix for BLAI_SUB, BV6_SUB and BMDR_SUB.